Available online at www.sciencedirect.com
SCIENCE DIRECT
Polymer 47 (2006) 1704–1714
polymer
www.elsevier.com/locate/polymer

Morphology and properties of melt-spun polycarbonate fibers containing single- and multi-wall carbon nanotubes

T.D. Fornes [a,b,1], J.W. Baur [a], Y. Sabba [a,b], E.L. Thomas [a,b,*]

[a] Institute for Soldier Nanotechnologies, Massachusetts Institute of Technology, 77 Massachusetts Avenue, Cambridge, MA 02139, USA
[b] Department of Materials Science and Engineering, Massachusetts Institute of Technology, 77 Massachusetts Avenue, Cambridge, MA 02139, USA

Received 19 August 2005; received in revised form 22 December 2005; accepted 3 January 2006
Available online 23 January 2006

Abstract

Polycarbonate fibers based single wall and multi-wall nanotubes (SWNT and MWNT) were prepared by first dispersing the nanotubes via solvent blending and/or melt extrusion followed by melt spinning the composites to facilitate nanotube alignment along the fiber axis. Morphological studies involving polarized Raman spectroscopy and wide angle X-ray scattering using a synchrotron radiation source show that reasonable levels of nanotube alignment are achievable. Detailed transmission electron microscopy (TEM) investigations on the polymer-extracted composite fibers reveal that MWNT more readily disperse within the PC matrix and have higher aspect ratios than do SWNT; extraction of the polymer from the composite prior to TEM imaging helps overcome the common issue of poor atomic contrast between the CNT and the organic matrix. Stress–strain analysis on the composites fibers show that MWNT, in general, provide greater stiffness and strength than those based on SWNT. Despite significant reinforcement of the polycarbonate, the level of reinforcement is far below what could be achieved if the nanotubes were completely dispersed and aligned along the fiber axis as predicted by composite theory.
© 2006 Elsevier Ltd. All rights reserved.

Keywords: Polycarbonate; SWNT; MWNT

1. Introduction

Carbon nanotubes (CNTs) are a new class of lightweight materials that posses extraordinary mechanical, electrical, and thermal properties. For example, the tensile modulus and strength of single and multiwalled nanotubes (SWNT and MWNT) have been estimated experimentally and theoretically to be of the order of 1 TPa and 30 GPa, respectively [1–4]. The combination of CNTs' low density, mechanical performance, and high aspect ratio make them excellent candidates for their use as fillers in high performance polymer nanocomposites. Such nanocomposites are attractive for their potential uses in aerospace and defense-related applications as well as in more conventional applications, e.g. automotive parts. However, full exploitation of the mechanical properties of CNTs in polymer composite applications will require exceptional control of dispersion and attainment of high degrees of alignment of individual tubes within the polymer matrix.

Significant progress is being made to address the issues of CNT dispersion and alignment. For example, surfactants and amphiphilic polymers, e.g. sodium dodecyl sulfate [5], sodium dodecylbenzene sulfonate [6,7], octylphenolethoxylate [8], poly(vinyl pryrollidone) [9], and Gum Arabic [10], are capable of dispersing low concentrations of SWNTs in solvents. Unfortunately, the low concentrations ($\ll 1\%$) and difficultly in removing the surfactant from the final product inhibit commercialization of this approach. More recent efforts in our laboratories [11,12] and elsewhere [13] have used moderately to highly acidic solutions, respectively, to disperse relatively high concentrations of SWNTs ($\sim$1–10 wt%) without the need of surfactants. A downside to strong acids is the tendency to degrade the nanotubes. The need for a more practical and environmentally conducive means of dispersing CNT within polymers have led researchers to evaluate direct melt processing of CNT–polymer mixtures, e.g. via twin screw extrusion, which has yielded promising results [14–18]. With regard to alignment, a number of approaches ranging from external magnetic fields [19,20] to electrospinning [21–24] to more conventional fiber spinning techniques [16,25–29] have been used to orient CNTs. Specifically, Hagenmuller et al. [25,30],

* Corresponding author. Address: Department of Materials Science and Engineering, Massachusetts Institute of Technology, 77 Massachusetts Avenue, Cambridge, MA 02139, USA. Tel.: +1 617 253 6901; fax: +1 617 2534119.
E-mail address: elt@mit.edu (E.L. Thomas).
[1] Present address: Lord Corporation, Chemical R&D, 110 Lord Dr., Cary NC 27512, USA.

0032-3861/$ - see front matter © 2006 Elsevier Ltd. All rights reserved.
doi:10.1016/j.polymer.2006.01.003

Sennett et al. [16], and Sreekumar et al. [27] reported high degrees of orientation of CNTs in melt-spun PMMA and PC fibers and dry–wet spun PAN fibers, respectively, as determined by polarized Raman spectroscopy, infrared spectroscopy, and transmission electron microscopy (TEM).

The aim of the present work is (i) to achieve good nanotube dispersion throughout the polymer matrix using solution and melt compounding methodologies, (ii) to promote nanotube alignment using the technique of fiber melt spinning, and (iii) to develop an understanding of the relationship between nanocomposite morphology and properties. Commercially available grades of SWNTs and multi-wall carbon nanotubes (MWNTs) have been incorporated into polycarbonate. Polycarbonate was chosen because of its good combination of stiffness and ductility, its ability to disperse CNTs via melt compounding, and because of its amorphous structure. An amorphous polymer was desired since fillers are well known to alter the crystalline morphology in semi-crystalline polymers which can complicate the interpretation of nanocomposite structure–property relationships.

2. Experimental section

2.1. Materials

Table 1 lists the materials used in this work. A high molecular weight grade of PC was chosen to generate high shear forces that could aid in the breakup and dispersion of the carbon nanotube bundles during melt compounding and to facilitate alignment during melt spinning of fibers. The higher molecular weight material also provides good melt strength and high levels of ductility which are needed when drawing fibers during melt spinning.

2.2. Melt processing

Fig. 1 shows the different processing routes used to form PC nanocomposites based on SWNTs and MWNTs. Nanocomposites containing SWNTs were formed from one of two routes, direct melt compounding (SWNT-dry) or solution blending followed by melt compounding (SWNT-soln). In the solution approach, SWNTs are first exfoliated in a 10 wt% solution of hydroxylamine hydrochloric acid salt (NH_2-$OH \cdot HCl$) in deionized water; the mechanism by which exfoliation occurs is believed to be an electrostatic repulsion caused by the adsorption of NH_3O^+ cations on the surfaces of individual carbon nanotubes that is capable of overcoming the van der Waals forces that holds the tubes together [11,12]. Following exfoliation, the salt is removed and water is replaced by THF through a series of washes. Next, a solution of PC and THF is added to the THF–SWNT solution. The PC–SWNT composite is then precipitated from solution using methanol and subsequently dried under vacuum at 120 °C. Explicit details of this solution dispersion technique can be found in a prior publication [11,12]. It was also of interest to compare nanocomposites derived from SWNTs to those derived from MWNTs made by direct melt compounding (Fig. 1). Studies by Sennett et al. [16] and Pötschke et al. [15] have revealed that MWNTs can be readily dispersed in molten PC using a twin screw extruder.

Melt compounding was carried out by recirculating PC–CNT blends containing 1, 3, and 5 wt% CNTs for 5 min in a counter-rotating, conical twin screw Haake Mini-Lab extruder operating at 285 °C and 100 rpm. Pelletized extrudate was placed inside an experimental-scale melt press spinner custom fabricated by DuPont that was further modified to spin small quantities of materials, i.e. $\lesssim 3$ cm^3. The material was then heated to 285 °C while under vacuum, and immediately extruded into fibers through a 381 μm diameter (D_0) single hole spinneret ($L/D_0 = 40$) at speeds yielding pressures of 700–1200 psig. A large L/D_0 spinneret was specifically chosen to promote alignment along the fiber axis. The extruded fiber was air cooled and drawn under tension at room temperature using a wind-up motor operating at speeds of 25 m/min or less to achieve a target diameter of $\sim$60 μm, corresponding to a target draw ratio, $\lambda = (D/D_0)^2$, of $\sim$40. Nanocomposites containing

Table 1
Materials used in forming polycarbonate–carbon nanotube composites

Material (designation used here)	Commercial designation	Comments/specifications	Supplier
Polymer			
Polycarbonate (PC)	Iupilon E2000	High viscosity grade $\bar{M}_n$[a] = 31,700 PDI[a] = 2.6	Mitsubishi Engineering Plastics
Carbon nanotubes			
Multi-walled carbon nanotubes (MWNT)		Length[b] = 1–5 μm Diameter[c] = 10 (±1.7) nm Fe content = 0.9 wt%[b]	Nanolab
Single-wall carbon nanotubes (SWNT)		Length[d] = 877 nm Diameter[e] = 1.1 (±0.02) nm Fe content = 0.2 wt%[f]	Carbon Nanotechnologies Inc.

[a] Molecular weight values and polydispersity index (PDI) determined via gel permeation chromatography.
[b] Information specified by the supplier.
[c] Determined by transmission electron microscopy.
[d] Number average length determined by atomic force microscopy measurements using surfactant dispersion techniques [41].
[e] Average diameter determined via Raman spectroscopy [41].
[f] Iron content determined by X-ray photoelectron spectroscopy [41].

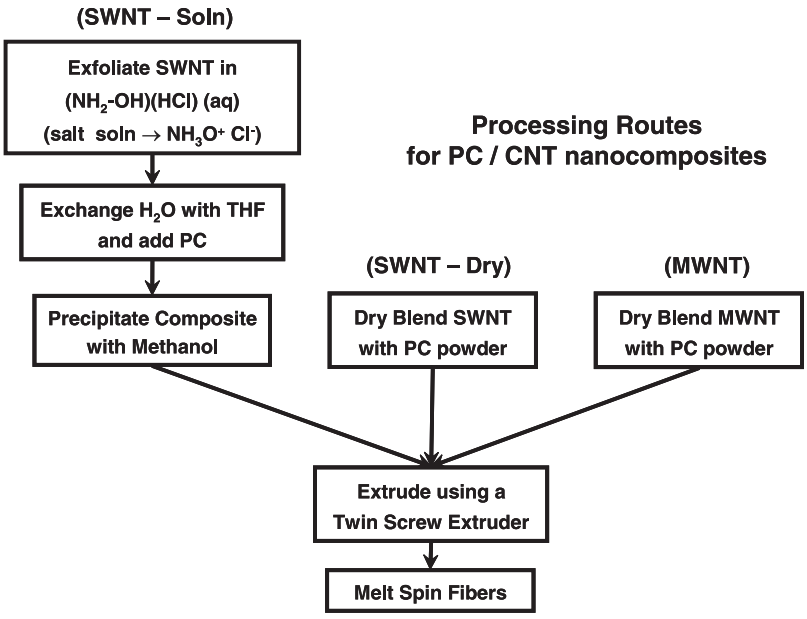

Fig. 1. Processing routes used to form PC nanocomposite fibers based on SWNT and MWNT.

5 wt% MWNT were limited to an average diameter of 89 μm ($\lambda = 18$) due to this material's low melt strength and, collectively, limited drawing ability. After melt spinning, all fibers were immediately sealed in a polyethylene bag and placed in a vacuum desiccator to prevent water uptake. Lastly, it should be noted that all materials containing PC were dried under vacuum at 120 °C for a minimum of 8 h prior to melt processing step.

2.3. Morphology characterization

Polarized Raman spectroscopy was used to assess the degree of orientation of SWNTs within PC fibers containing 5 wt% SWNT; Raman spectra were collected for 30 s using a Kaiser Hololab 5000R Microscope using a 785 nm excitation laser (0.70 mW) configured in the VV geometry where the polarizer and the analyzer were parallel to each other, and at discrete angles between 0 and 90° relative to the fiber axis. The fiber axis was rotated with the polarizer/analyzer fixed.

Wide angle X-ray diffraction (WAXD) experiments were conducted at the synchrotron X-ray beamline X27C of the National Synchrotron Light Source in Brookhaven National Laboratory. The wavelength of the X-ray beam was 0.137 nm. The sample-to-detector distance was 84.8 mm, as determined by calibration using a α-Al_2O_3 standard. X-ray patterns obtained from yarns comprised of approximately 10 fibers were collected on image plates for a period of 10 min. The patterns were converted into digital format and analyzed using Polar and FIT2D software, respectively.

TEM was used to evaluate the degree of CNT dispersion within the PC matrix. To overcome the issue of poor contrast between CNTs and the polymer matrix, the polymer was extracted from the composite prior to TEM imaging using the following technique: filter paper was stacked inside a glass Petri dish. Chloroform was added to a level just below the top portion of the filter paper, yet still allowing for saturation of the stack. Lacey carbon grids (300 mesh) were placed on top of the filter paper. Small pieces of nanocomposite fiber approximately 1 mm in length were then placed on top of the grids. The assembly was covered and allowed to sit for a minimum of 24 h. A beaker of excess chloroform was placed inside the chamber to provide a saturated environment in order to minimize the depletion of the solvent within the Petri dish by evaporation. The resulting polymer-extracted samples were examined at an accelerating voltage of 120 kV using a JEOL 200CX TEM. Higher magnification images were also recorded using a JEOL 2010 TEM with a LaB_6 filament operating at an accelerating voltage of 200 kV. In addition to analyzing extracted samples, TEM analyses were conducted on microtomed sections cut from the central portion of PC/5 wt% MWNT fibers. Ultra thin sections approximately 50 nm in thickness were cut perpendicular to the fiber axis at room temperature with a diamond knife at using a Reichert-Jung Ultracut E microtome.

2.4. Property testing

Fiber tensile properties were measured with a Zwick Z010 Materials Testing Machine using a 10 N load cell, a crosshead speed of 5.1 mm/min, and a fiber gauge length of 25.4 mm. Prior to testing, fibers were mounted on sturdy paper frames using a high-strength epoxy adhesive and placed in a desiccator for a minimum of 24 h. Diameter measurements were made in three equally spaced locations along the gauge length of each specimen using an optical microscope.

3. Results

3.1. Nanocomposite morphology

Various analytical methods can be used to determine the microstructure of the composites. For SWNTs, polarized Raman spectroscopy works well, while wide angle X-ray scattering can be used only on the MWCNTs. TEM is a challenge for both types of samples. Fig. 2 shows polarized Raman spectra for PC fibers containing SWNT-soln and SWNT-dry obtained at various fiber angles, ψ, relative to the polarization direction. Each set of spectra exhibits peaks at frequencies between $\sim$160–265 cm^{-1} and at $\sim$1310 and $\sim$1588 cm^{-1}, corresponding to the vibrational modes of SWNTs [31,32], i.e. the radial breathing mode, disordered-induced D-band, and tangential mode or G-band, respectively. Large decreases in the intensity of the peaks are observed when the fiber is rotated from parallel ($\psi = 0°$) to perpendicular ($\psi = 90°$) to the polarization direction which suggests some degree of SWNT orientation along the fiber axis. This effect may be better visualized by plotting the normalized Raman peak intensity versus fiber angle, as shown in Fig. 3 for the 1588 cm^{-1} peak. Included in Fig. 3 is the theoretical curve for perfectly aligned SWNT, where intensity is proportional to

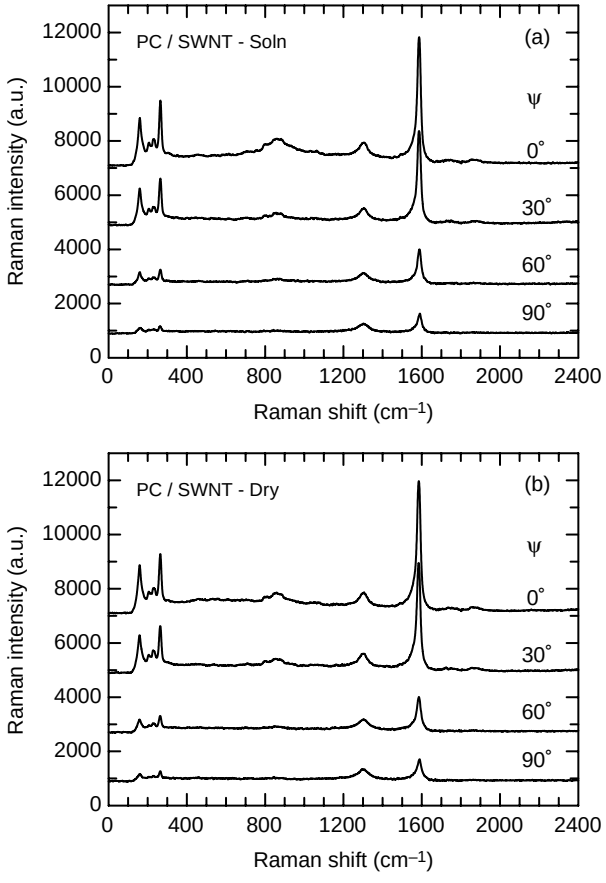

Fig. 2. Polarized Raman spectra of melt-spun PC nanocomposite fibers based on (a) SWNT-soln and (b) SWNT-dry taken at various fiber angles, ψ, relative to the incident polarization. Each sample contains 5 wt% SWNT. Spectra have been shifted vertically for clarity.

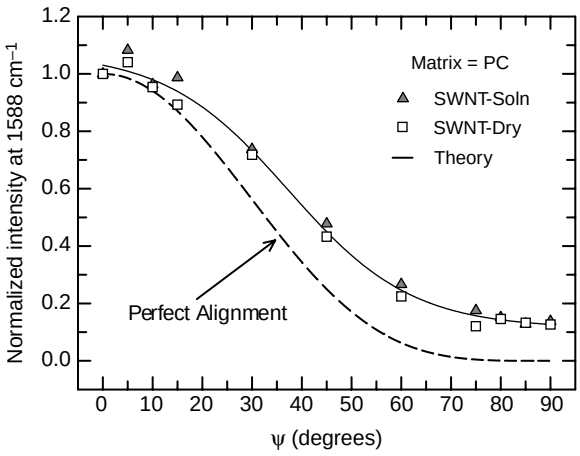

Fig. 3. The effect of fiber angle, ψ on the normalized Raman intensity at 1588 cm^{-1} (tangential mode or G-band) for melt-spun PC nanocomposite fibers based on SWNT-soln and SWNT-dry. The lower dashed line represents the relationship between relative intensity and fiber angle for perfect or unidirectional alignment of SWNT along the fiber axis.

$\cos^4\psi$. The dependency of the normalized Raman intensity on fiber angle is nearly identical for the two preparations of the PC–SWNT nanocomposites, indicating comparable degrees of SWNT alignment along the fiber axis.

Curve fits to the data in Fig. 3 yield quantitative information on the degree of alignment of the SWNT along the fiber axis. The intensity of a Raman peak at a given angle, ψ, between the fiber and polarization axes, can be represented by

$$I_{\text{fiber}}(\psi) = \int_{\psi-\pi/2}^{\psi+\pi/2} cF(\theta-\psi,\Delta)\cos^4\theta \,\mathrm{d}\theta \tag{1}$$

where θ is the angle between the SWNT axis and the incident excitation polarization, c is a parameter that gives the maximum intensity when $\theta = 0$, and F is a function that describes the orientation distribution of the SWNTs. For SWNT orientation that follows a Lorentzian distribution, the function F is represented by the following form:

$$F(\theta-\psi,\Delta) = \frac{\Delta/2\pi}{(\theta-\psi)^2-(\Delta/2)^2} \tag{2}$$

The parameter Δ is the FWHM of the distribution. Performing a least of squares fit of Eqs. (1) and (2) to the experimental data in Fig. 3 yields a best fit value of $\Delta = 12°$ for both SWNT-soln and SWNT-dry based nanocomposites. This model has been used by Haggenmuller et al. [25] to assess the degree of SWNT orientation within melt spun PMMA fibers. They report Δ values of 4 and 23° for fibers having a high and low draw ratio, respectively.

WAXD analyses were conducted to assess the degree of alignment of MWNT within nanocomposites. Fig. 4 shows X-ray patterns taken of fiber yarns of pure PC (Fig. 4(a)) and its corresponding nanocomposite (Fig. 4(b)) containing 5 wt% MWNT with the incident beam is perpendicular to the fiber axis. At least two reflections are present in both patterns, an intense broad reflection corresponding to the average spacing

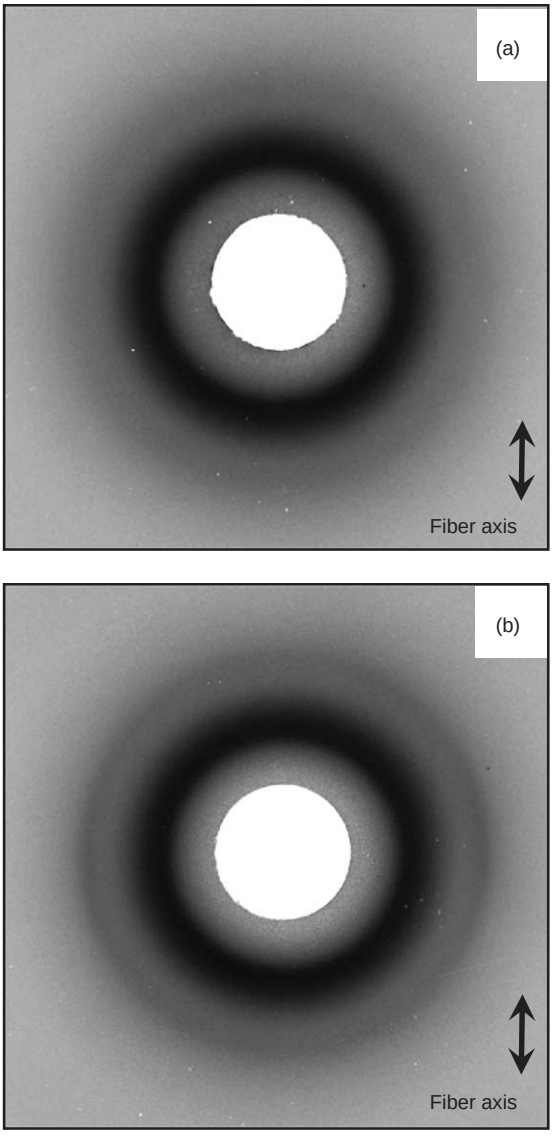

Fig. 4. WAXD diffraction patterns of (a) pure PC fiber yarns and (b) PC nanocomposite fiber yarns containing 5 wt% MWNT obtained using synchrotron X-ray radiation.

of amorphous polycarbonate chains (inner peak) and a less intense, outer somewhat narrower peak. Integrating the intensity over the entire 2D space as function of 2θ provides a better indication of the different intensity distributions as shown in Fig. 5. The less intense outer peak in Fig. 4(a) is represented by a small shoulder present at $2\theta \cong 23.3°$ ($d \cong 0.340$ nm) in Fig. 5. On the other hand, the nanocomposite exhibits a more intense reflection located at a slightly lower 2θ value of $\sim 22.5°$ ($d \cong 0.345$ nm). This reflection is likely a superposition of two peaks, one corresponding to the pure polycarbonate, the other corresponding to the average spacing between graphitic sheets that comprise the MWNT, $d_{002} \cong 0.345$ nm. Subtracting the pure PC pattern from the nanocomposite pattern in Fig. 4 yields a pattern containing scattering solely from the MWNT as shown in Fig. 6(a). The subtracted pattern has strong equatorial d_{002} reflections perpendicular to the fiber axis which indicates that the

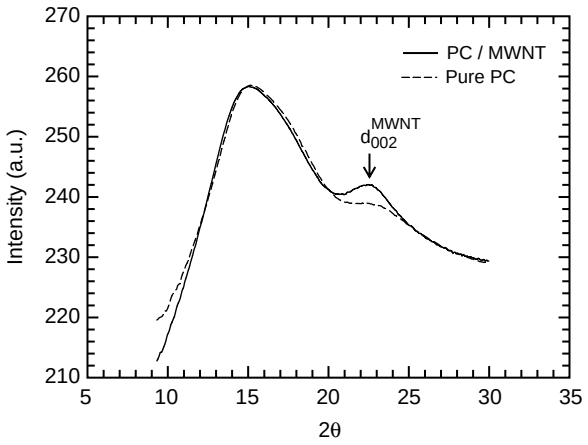

Fig. 5. Intensity versus 2θ plot obtained from 2D integration of diffraction patterns shown in figure for a melt-spun PC fibers and its corresponding nanocomposite containing 5 wt% MWNT.

MWNT prefer to orient along this axis. The azimuthal scan of the d_{002} reflection presents a more quantitative picture of the orientation of the filler. Both peaks exhibit full width at the half intensity maximums (FWHM) of $\sim 56°$, indicating a moderate degree of alignment of the filler along the fiber axis.

TEM analyses on the three types of PC nanocomposites lend insight into the level of CNT dispersion within the PC matrix. To circumvent the issue of poor contrast between the CNTs and

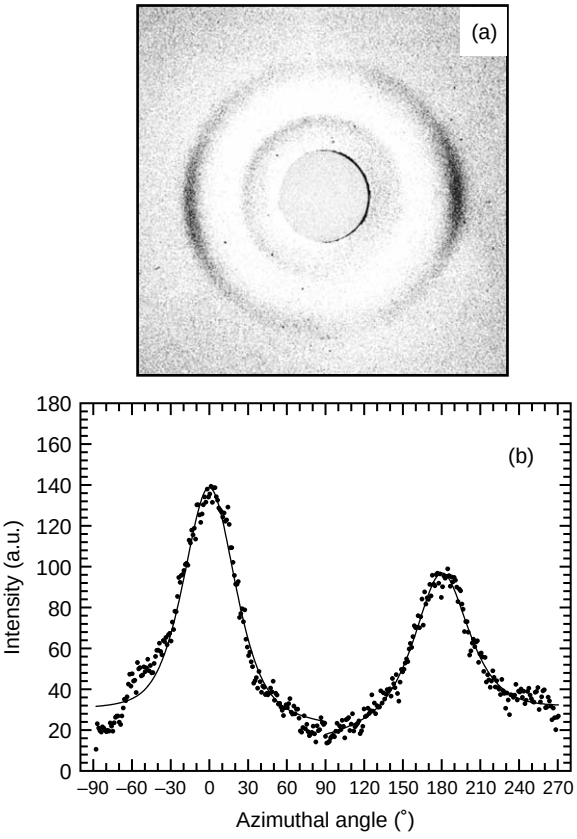

Fig. 6. (a) WAXD pattern obtained from subtraction of the pure PC pattern from the nanocomposite pattern in Fig. 5(b). Intensity of the MWNT d_{002} reflection as function of azimuthal angle. The dark lines represent a best fit curve based on Gaussian–Lorentzian distribution.

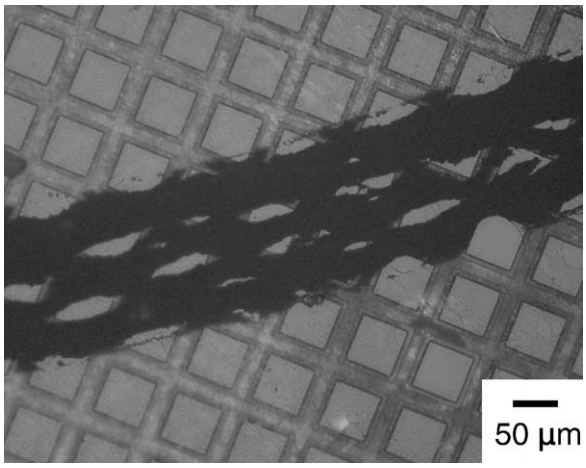

Fig. 7. Optical photomicrograph of a PC nanocomposite fiber on a lacey-carbon grid following matrix extraction with chloroform.

polymer matrix, the polymer was extracted from the fiber prior to TEM imaging, thereby, leaving a collapsed array of CNTs. Fig. 7 is an optical photomicrograph of an extracted fiber obtained using the technique described earlier. TEM photomicrographs of extracted fibers containing 5 wt% CNT are shown in Fig. 8. Photomicrographs of SWNT-soln and SWNT-dry based nanocomposites in Fig. 8(a) and (b) have a similar morphology which consists of a distribution of long SWNT particles. The particles are comprised predominately of ropes or bundles of SWNTs ranging from a few nanometers to tens of nanometers in thickness. In addition, there are regions of undissolved polymer or amorphous carbon as well as remnants of dark, dense round particles, likely corresponding to Fe-catalyst particles left over from the synthesis of the pristine SWNTs. It appears that the polymer extraction method tends to favor retention of large area tube networks where entanglements are more pronounced, rather than lightly aligned regions. It is likely that single SWNTs are not retained in this method of sample preparation. Higher magnification photomicrographs in Fig. 9 provide greater detail of crystalline rope structures. Fig. 9(b), an enlarged section of Fig. 9(a), shows ropes having discernable individual nanotube features. Contrary to the SWNT nanocomposites, the morphology of MWNT nanocomposite is more uniform, consisting primarily of individual nanotubes (Fig. 8(c)).

Image analyses conducted on TEM photomicrographs provide comparisons of the final CNT particle diameters for the three types of composites as shown in Fig. 10. The histograms for the SWNT based nanocomposites exhibit a broad range of particle diameters and yield comparable average values. The histogram for the MWNT nanocomposite is much more compact and the average diameter is slightly less than that of the SWNT materials. This is due to the fact that the measured final particle diameters for MWNT particles values reflect dimensions of individual nanotubes rather than the diameters of ropes of tube bundles as encountered in the SWNT composites.

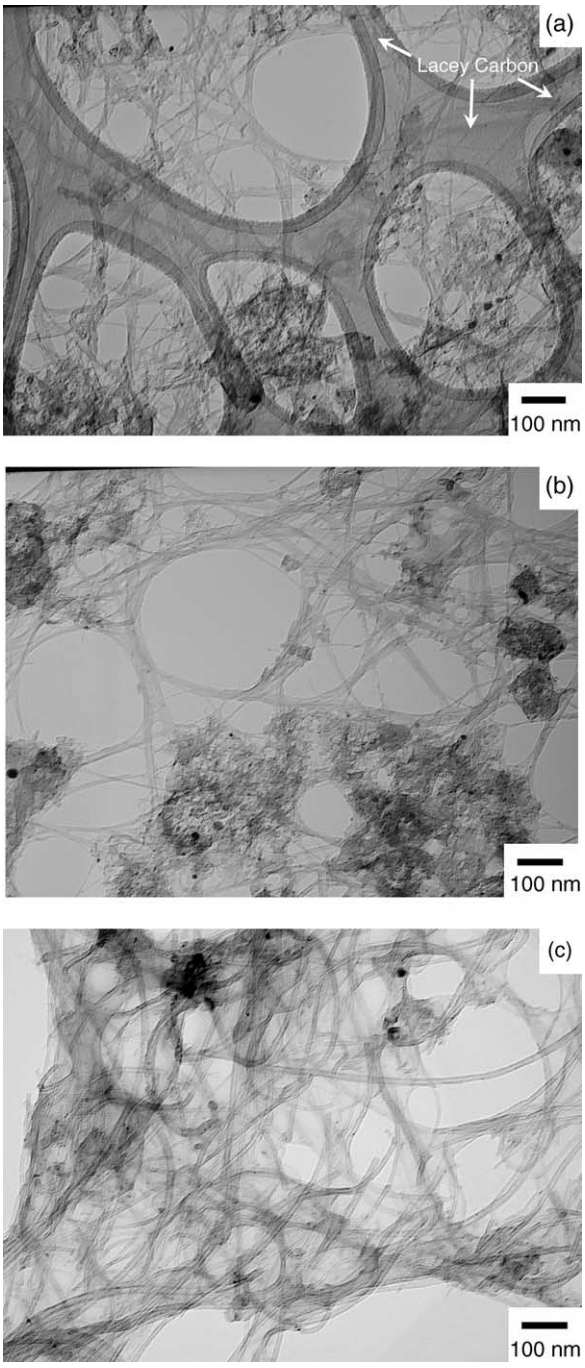

Fig. 8. TEM photomicrographs of extracted PC nanocomposite fibers based on (a) SWNT-soln, (b) SWNT-dry, and (c) MWNT. Each composite contains 5 wt% CNT.

3.2. Nanocomposite properties

Table 2 summarizes the mechanical of melt-spun PC nanocomposite fibers based on MWNT, SWNT-soln, and SWNT-dry. Fig. 11 shows the influence of MWNT concentration on the stress–strain behavior of nanocomposite fibers. Adding MWNT results in an increase in modulus and yield strength and a sacrifice in ductility. Interestingly, samples with and without nanotubes exhibited multiple neck formation immediately following the yield point, eventually forming

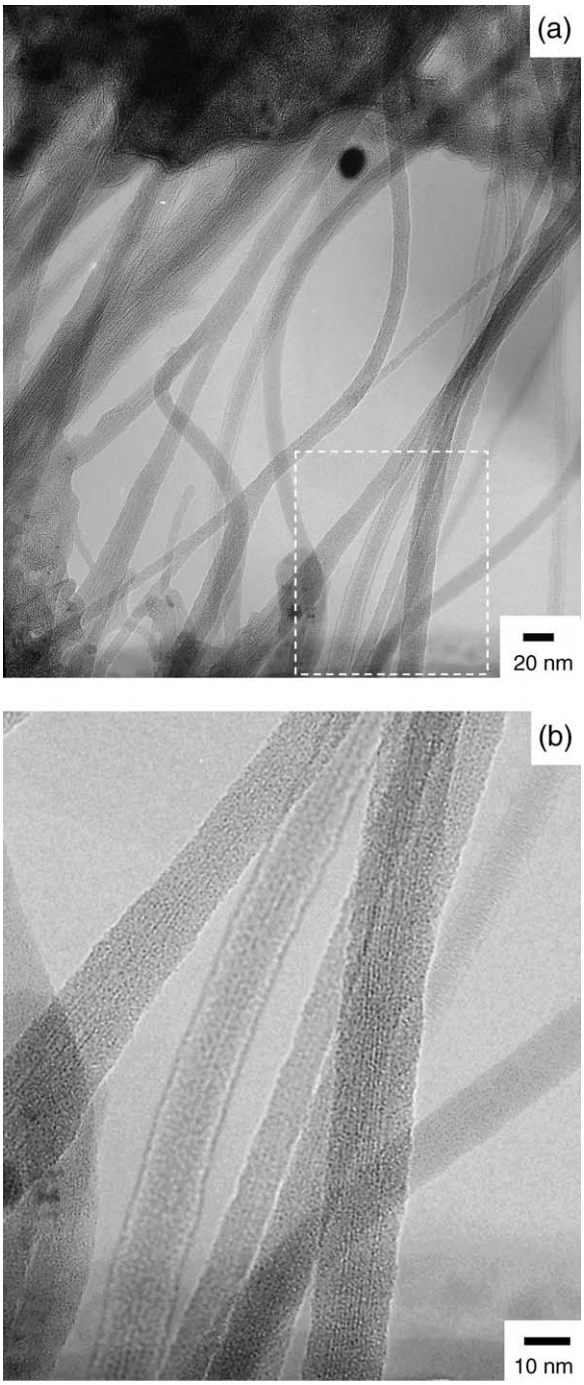

Fig. 9. High resolution TEM photomicrographs of extracted PC nanocomposite fibers based on SWNT-soln. (b) Corresponds to the rectangular region highlighted in (a).

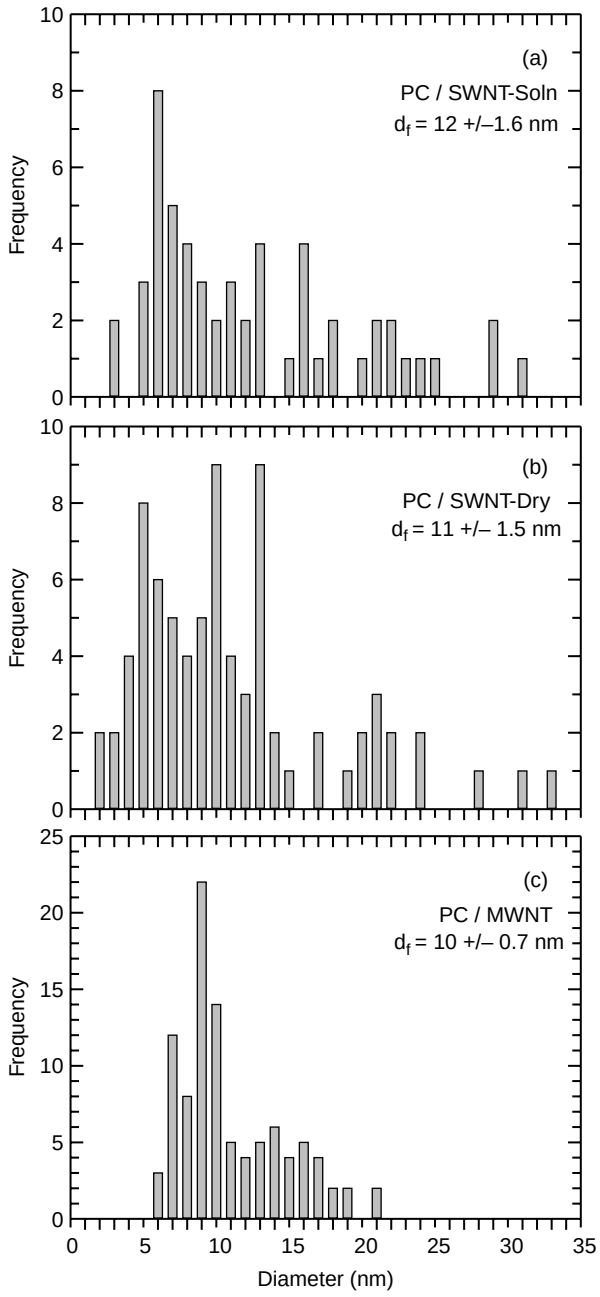

Fig. 10. Histograms of final particle diameters obtained from image analyses of TEM photomicrographs of PC nanocomposites based on (a) SWNT-soln, (b) SWNT-dry, and (c) MWNT.

a stable neck at higher elongations. Moreover, this behavior was more pronounced in the nanocomposites samples. Similar stress–strain behavior is also observed in nanocomposites based on SWNT-soln and SWNT-dry, but the stiffness, yield strength, and ultimate strain to break are affected by CNT concentration to different degrees.

The effect of CNT concentration on nanocomposite modulus is shown in Fig. 12(a). Included in this plot are theoretical curves generated using the theory of Halpin–Tsai [33,34] that represent the ultimate stiffness expected if the CNTs were completely exfoliated, dispersed, and perfectly aligned along the fiber axis. Experimentally, the three types of nanocomposites exhibit comparable moduli at CNT concentrations up to 3 wt%. Beyond this concentration, nanocomposites based on MWNT have significantly higher moduli than those based on SWNT-soln and SWNT-dry. Similar trends are observed in the plot of yield strength versus weight percent CNT as shown in Fig. 12(b). For the MWNT nanocomposites, the yield strength increases steadily with weight percent CNT over the concentrations examined; whereas, nanocomposites based on both SWNT-soln and SWNT-dry show an initial rise

Table 2
Tensile and electrical properties of PC nanocomposite fibers based on MWNT, SWNT-soln, and SWNT-dry

Wt% CNTs	Diameter[a] (μm)	Modulus[a] (GPa)	Yield strength[a] (MPa)	Elongation at break[a] (%)
Pure PC				
0	65 (±2.2)	1.82 (±0.11)	43.0 (±2.5)	>140[b]
PC/MWNT				
1	65 (±2.3)	2.20 (±0.21)	52.8 (±1.4)	>140[b]
3	68 (±1.4)	2.54 (±0.50)	60.1 (±2.1)	80 (±23)
5	89 (±2.5)	3.12 (±0.20)	63.9 (±3.4)	47 (±8)
PC/SWNT-soln				
1	62 (±1.2)	2.20 (±0.11)	54.3 (±2.0)	>140[b]
3	60 (±1.7)	2.41 (±0.15)	53.4 (±2.2)	139 (±8)
5	61 (±2.0)	2.77 (±0.12)	56.4 (±1.6)	96 (±8)
PC/SWNT-dry				
1	64 (±0.7)	2.19 (±0.06)	50.5 (±3.0)	>140[b]
3	52 (±3.2)	2.52 (±0.26)	49.7 (±3.1)	113 (±12)
5	64 (±1.9)	2.71 (±0.20)	52.2 (±1.7)	104 (±18)

[a] Error values reported are based on a 95% confidence interval.
[b] Samples under high strains were prone to slipping at the epoxy-fiber interface due to necking of the fiber within the epoxy adhesive.

in yield strength up to 1 wt%, followed by a plateau in strength that is significantly below that the PC–MWNT values.

4. Discussion

The above results indicate that reasonable levels of CNT dispersion and alignment can be achieved using solution and melt compounding methodologies combined with fiber melt spinning. With regard to nanotube alignment, analyses on Raman spectra and WAXD patterns confirm quantitatively that intermediate levels of CNT orientation are achieved along the fiber axis. However, because SWNTs do not give a recognizable wide angle X-ray signal, and MWNTs do not provide useful Raman data for determining nanotube orientation, and thus a rigorous comparison of the relative orientation of each type of carbon nanotube is not possible.

Morphological results obtained via TEM clearly show that individual MWNT are much easier to disperse than individual

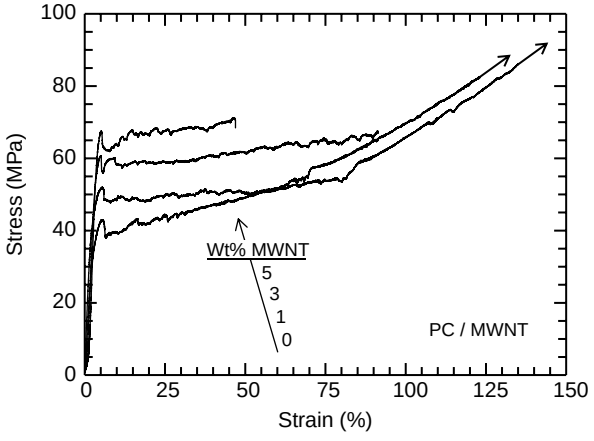

Fig. 11. The effect of CNT content on the stress–strain behavior of melt-spun PC fibers and MWNT nanocomposites thereof.

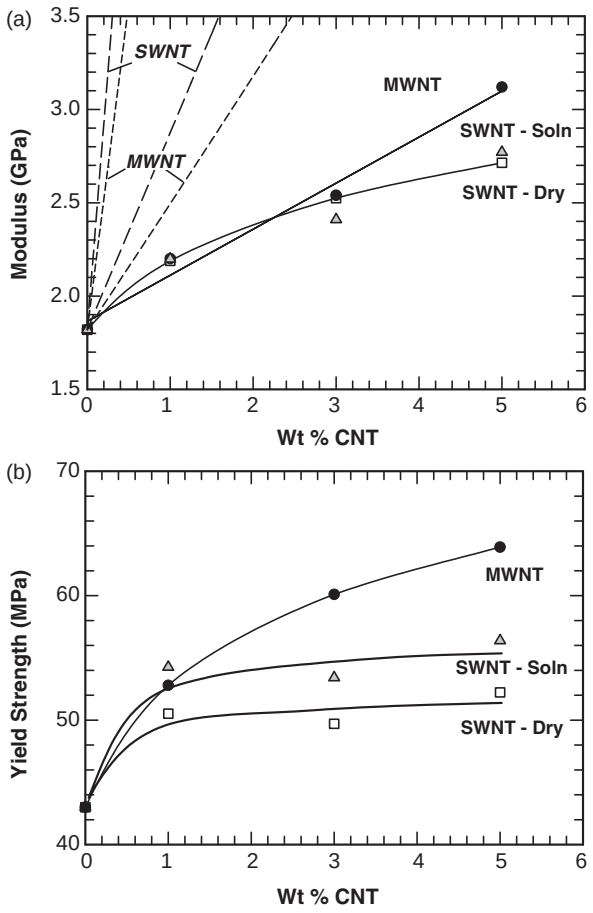

Fig. 12. The effect of CNT content on (a) modulus and (b) yield strength of melt-spun PC nanocomposites fibers based on MWNT, SWNT-soln, and SWNT-dry. Ideal curves shown in (a) are based on a matrix modulus, E_m, of 1.82 GPa, a filler modulus, $E_{CNT} = 1.0$ TPa, and the assumption that the filler is completely dispersed and either fully aligned with respect to the applied load (left dashed curves) or randomly oriented in all three directions (right dashed curves).

SWNT, regardless of the processing route used to fabricate the SWNT based nanocomposites. Similar findings have been reported by Sennett et al. [16] for melt processed nanocomposites. A major limitation toward complete exfoliation of individual SWNT is due to their small diameters and their propensity to pack efficiently into ropes during their synthesis. In order for the polymer to exfoliate the tubes comprising the ropes, it must diffuse within the space between neighboring tubes of the rope either from the ends and/or sides. To accomplish this, the polymer must undergo large configurational changes from its naturally coiled state, which is entropically unfavorable. The entropic penalty incurred by the deformation of the polymer chain will depend on the size of the space available which is inversely proportional to the diameter of the nanotubes.

The diameter of the space between the individual tubes or channel diameter is about 15% of the tube's diameter. The diameter of 1.1 nm for the SWNTs used in this work corresponds to a channel diameter of ~0.17 nm. This value is nearly two orders of magnitude less than the radius of

gyration for the present PC which is estimated to be ~13 nm [35,36], suggesting that polymer is essentially incapable of inter-diffusion into the ropes comprised of single wall tubes. Therefore, based on diffusion alone, exfoliation of the small diameter nanotubes, unlike MWNTs, is geometrically limited by polymer melts. Of course, there are number of additional factors besides diffusion that govern the exfoliation of CNTs, such as rheological effects, imperfect packing of tubes, structural defects, etc. Clearly, more work needs to be done to better understand the mechanisms governing nanotube exfoliation.

The differences in the level of CNT dispersion and resulting filler particle dimensions between the different nanocomposites may explain the mechanical property trends observed in Fig. 12. It is well known that higher aspect ratio fillers will naturally impart greater reinforcement of the polymer matrix than lower ones. The final filler aspect ratio for CNT particles will depend on the inherent size of the pristine, individual nanotubes and extent of nanotube dispersion. Image analyses of TEM photomicrographs reveal very similar average final particle diameters for the three different nanocomposites, i.e. ~10 nm for the MWNTs nanocomposites, ~12 nm for the SWNT-soln nanocomposites, and ~11 nm for the SWNT-dry nanocomposites. Although final particle lengths ($\bar{\ell}_f$) are unattainable from TEM photomicrographs, it is reasonable to assume that the average aspect ratio of the MWNT particles, $(\bar{\ell}_f/\bar{d}_f)_{MWNT}$, is considerably higher than that of the SWNT particles since the inherent average length ($\bar{\ell}_0$), of the pristine, individual MWNTs are greater than the corresponding SWNT average length (Table 1). Substituting ($\bar{\ell}_0$) for ($\bar{\ell}_f$) provides gives a rough estimate of aspect ratio, i.e.

$$\left(\frac{\bar{\ell}_0}{\bar{d}_f}\right)_{MWNT} \sim 300, \quad \left(\frac{\bar{\ell}_0}{\bar{d}_f}\right)_{SWNT-soln} \sim 70, \quad \text{and}$$

$$\left(\frac{\bar{\ell}_0}{\bar{d}_f}\right)_{SWNT-dry} \sim 80.$$

It is also important to comment on the absolute stiffness and yield strength values of the nanocomposites. For example, the moduli and yield strength of nanocomposites containing 5 wt% MWNT exhibit a 75 and 50% increase, respectively, relative to that of pure polycarbonate. These improvements fall within the range of mechanical property enhancements encountered in other polymer–CNT composite fibers, such as those based on poly(methyl methacrylate) [17,25], polyacrylonitrile [27], polyamide 12 [28], and poly(*p*-phenylene benzobisoxazole) [26]. Moreover, these results demonstrate the utility of CNTs since the level reinforcement of PC by CNTs is considerably more efficient than what is achieved by conventional fillers, e.g. glass fibers, and nano-sized clay, e.g. montmorillonite [37]. Nevertheless, the results still fall well short of what can ultimately be achieved as predicted by composite theory (see ideal curves in Fig. 12(a)). The large discrepancy between experiment and theory stems from a number of likely factors: incomplete nanotube exfoliation, incomplete alignment of the nanotubes along the fiber axis, and the presence of considerable

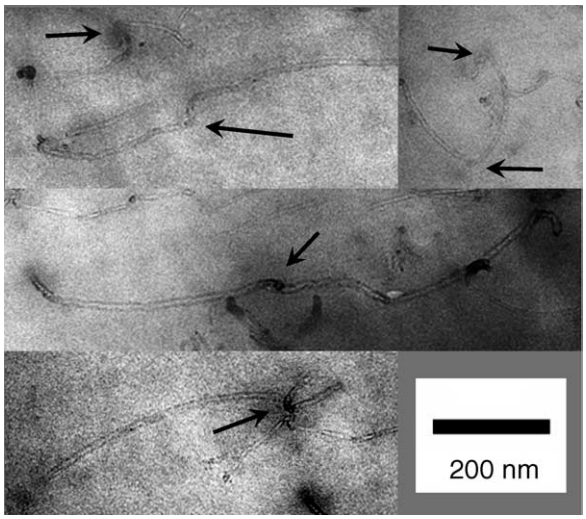

Fig. 13. TEM photomicrographs of microtomed sections of PC/MWNT fibers showing evidence of twist like defects (black arrows) present in individual MWNT.

defects and impurities in the raw nanotube products. The latter issue is of particular concern. Defects such as kinks, twists, voids, pentagon and heptagonal inclusions are expected to have a detrimental impact on the mechanical properties of the nanotube [31,38]. Impurities, like amorphous carbon, which is prevalent in significant amounts in commercially available CNTs, tend to coat the nanotubes and thereby reduce the strength of the polymer–nanotube interface. TEM photomicrographs of the present PC/MWNT composites shown in Fig. 13 provide experimental evidence of twist-like defects within the MWNT.

There are several ways to improve the mechanical properties of PC–CNT nanocomposites. An obvious route toward improvement is increasing the draw ratio of the melt-spun fiber. This will impart greater extensional stresses on the CNTs, thereby improving CNT alignment along the fiber axis, which ultimately allows the filler to carry a larger amount of the applied load. Studies by Haggenmuller et al. [25,39] have indeed demonstrated that improved alignment of SWNT in PMMA and polyethylene fibers and corresponding increases in nanocomposite moduli are achievable by increasing the fiber draw ratio. Functionalization of CNTs also offers the promise of improving mechanical properties by improving stress transfer between the nanotube and polymer matrix thorough chemical bonds rather than physical bonds. In addition, functionalization may aid in nanotube dispersion due to increased CNT–polymer compatibility. However, it is unclear at this point how the properties of the nanotubes are affected by the functionalization process. As highlighted by Wagner and Vaia [40], only a limited amount of research has been devoted toward understanding the properties of polymer–CNT interfaces.

A not so obvious route toward improving the mechanical properties of PC–CNTs is to use nanotubes having smaller length than commercially available nanotubes. There is a strong tendency in the literature to overemphasize the positives of having high aspect ratio nanotubes. Indeed, exfoliating and

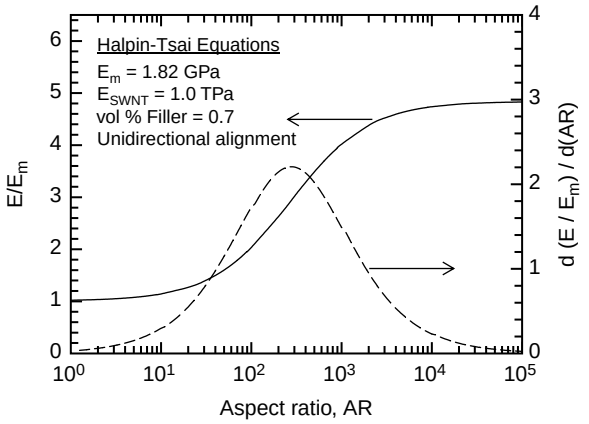

Fig. 14. The influence of SWNT aspect ratio on the longitudinal reinforcement of PC and its corresponding derivative predicted using the theory of Halpin–Tsai. Calculations are based on a matrix modulus, E_m, of 1.82 GPa, a filler modulus, E_{SWNT} = 1.0 TPa and the assumption that the SWNT are completely dispersed and aligned relative to the applied load.

dispersing large aspect ratio nanotubes within polymers will, in theory, result in superior mechanical and electrical properties at extremely low filler levels. However, a tradeoff of using very long and flexible nanotubes is the formation of large bundles or nests of nanotubes that are result of the large number of tube entanglements. Unfortunately, it is extremely difficult to completely disentangle, disperse, and align the individual nanotubes upon incorporation into polymer matrices, which are essential steps for fully exploiting the nanotube's reinforcing ability. Another point often not taken into account is that the level of stiffness enhancement experienced in polymer–CNT nanocomposites becomes less efficient beyond a certain nanotube length (or aspect ratio, AR). This effect is shown in Fig. 14 which shows a plot of relative modulus of PC nanocomposites containing 0.7 vol% (~1 wt%) SWNT as a function of nanotube aspect ratio; the calculations assume complete nanotube exfoliation and alignment with respect to the applied load. The mechanical property benefit of having higher aspect ratio particles begins to diminish beyond an aspect ratio of ~300 which is evident in the derivative of the E/E_m versus AR curve. As the aspect ratio approaches ~2000, E/E_m becomes virtually insensitive to aspect ratio and follows a rule of mixtures type behavior. Interestingly, commercial SWNTs are commonly supplied in lengths ranging between 1 and 5 μm, corresponding to aspect ratios of the individual tubes of ~1000–5000. Given this information and the aforementioned comments with regard to entanglements, it seems more advantageous from a mechanical property standpoint to use nanotubes with individual aspect ratios nearly one third to half of typical commercial product. Such dimensions would make it easier to disentangle, disperse, and subsequently align the nanotubes within the polymer matrix.

A final comment is warranted on the morphology on the morphology and properties of SWNT-soln nanocomposites versus SWNT-dry nanocomposites. It was originally expected that dispersing SWNTs in PC via solution blending prior to melt processing would lead to better dispersion and nanocomposite properties than dry blending alone. However, results indicate that there is no significant difference in the morphology and properties obtained using the different fabrication routes. This is encouraging from a commercial standpoint, since many polymeric materials are exposed to some form of melt processing in order to form the material into a useful shape. Nevertheless, both techniques are still limited in their ability to completely exfoliate ropes of SWNT nanotubes as indicated by the final particle diameters. Further investigations aimed at understanding the effects of nanotube diameter on nanotube dispersion would help address this issue.

5. Conclusions

Polycarbonate composite fibers containing SWNT and MWNT were fabricated by first dispersing the nanotubes by solvent blending and/or melt extrusion followed by melt spinning the composites to promote tube alignment along the fiber axis. MWNT were found to more readily disperse within the PC matrix and have larger particle aspect ratios than SWNT as determined by transmission electron microscopy; careful extraction of the PC matrix prior to TEM investigations helped circumvent the issue of poor image contrast commonly encountered when performing electron microscopy of CNTs in organic matrices. The extent of nanotube dispersion is believed to be governed, in part, by the matrix polymer's ability to break up neighboring nanotubes. Larger diameter nanotubes pose less entropic constraints on interparticle diffusion by the polymer. The level of mechanical reinforcement was in accord with morphological findings in that MWNT composites exhibited higher moduli and yield strengths than those based on SWNT. Despite significant increased mechanical reinforcement, the level of reinforcement falls well below that if the nanotubes were fully dispersed and aligned along the fiber axis as predicted by composite theory.

Acknowledgements

The authors Dr Vaughn Samuelson and James O'Connor of DuPont for their assistance with the initial setup of the melt press spinner, and Prof Robert E. Cohen of MIT for the use of the Haake Mini-Lab extruder. This material is based upon work supported by, or in part by, the US Army Research Laboratory and the US Army Research Office under contract DAAD-19-02-D-0002.

References

[1] Treacy MMJ, Ebbesen TW, Gibson JM. Nature (London) 1996;381:678.
[2] Yu M-F, Files BS, Arepalli S, Ruoff RS. Phys Rev Lett 2000;84:5552.
[3] Wong EW, Sheehan PE, Lieber CM. Science 1997;277:1971.
[4] Yakobson BI, Avouris P. Top Appl Phys 2001;80:287.
[5] Vigolo B, Penicaud A, Coulon C, Sauder C, Pailler R, Journet C, et al. Science 2000;290:1331.
[6] Islam MF, Rojas E, Bergey DM, Johnson AT, Yodh AG. Nano Lett 2003; 3:269–73.
[7] Paredes JI, Burghard M. Langmuir 2004;20:5149.
[8] Wang H, Zhou W, Ho DL, Winey KI, Fischer JE, Glinka CJ, et al. Nano Lett 2004;4:1789.

[9] O'Connell MJ, Boul P, Ericson LM, Huffman C, Wang Y, Haroz E, et al. Chem Phys Lett 2001;342:265.
[10] Bandyopadhyaya R, Nativ-Roth E, Regev O, Yerushalmi-Rozen R. Nano Lett 2002;2:25.
[11] Sabba Y, Thomas EL. Macromolecules 2004;37:4815.
[12] Sabba Y, Thomas EL. Macromolecules 2004;37:6662.
[13] Davis VA, Ericson LM, Parra-Vasquez ANG, Fan H, Wang Y, Prieto V, et al. Macromolecules 2004;37:154.
[14] Potschke P, Fornes TD, Paul DR. Polymer 2002;43:3247.
[15] Potschke P, Bhattacharyya AR, Janke A. Eur Polym J 2003;40:137.
[16] Sennett M, Welsh E, Wright JB, Li WZ, Wen JG, Ren ZF. Appl Phys A: Mater Sci Process 2003;76:111.
[17] Gorga RE, Cohen RE. J Polym Sci, Part B: Polym Phys 2004;42:2690.
[18] Liu T, Phang IY, Shen L, Chow SY, Zhang W-D. Macromolecules 2004; 37:7214.
[19] Smith BW, Benes Z, Luzzi DE, Fischer JE, Walters DA, Casavant MJ, et al. Appl Phys Lett 2000;77:663.
[20] Fischer JE, Zhou W, Vavro J, Llaguno MC, Guthy C, Haggenmueller R, et al. J Appl Phys 2003;93:2157.
[21] Dror Y, Salalha W, Khalfin RL, Cohen Y, Yarin AL, Zussman E. Langmuir 2003;19:7012.
[22] Ko F, Gogotsi Y, Ali A, Naguib N, Ye H, Yang G, et al. Adv Mater 2003; 15:1161.
[23] Sen R, Zhao B, Perea D, Itkis ME, Hu H, Love J, et al. Nano Lett 2004;4: 459.
[24] Hou H, Reneker DH. Adv Mater 2004;16:69.
[25] Haggenmueller R, Gommans HH, Rinzler AG, Fischer JE, Winey KI. Chem Phys Lett 2000;330:219.
[26] Kumar S, Dang TD, Arnold FE, Bhattacharyya AR, Min BG, Zhang X, et al. Macromolecules 2002;35:9039.
[27] Sreekumar TV, Liu T, Min BG, Guo H, Kumar S, Hauge RH, et al. Adv Mater 2004;16:58.
[28] Sandler JKW, Pegel S, Cadek M, Gojny F, van Es M, Lohmar J, et al. Polymer 2004;45:2001.
[29] Ericson LM, Fan H, Peng H, Davis VA, Zhou W, Sulpizio J, et al. Science 2004;305:1447.
[30] Hwang J, Gommans HH, Ugawa A, Tashiro H, Haggenmueller R, Winey KI, et al. Phys Rev B: Condens Matter Phys 2000;62:R13310.
[31] Dresselhaus MS, Dresselhaus G, Avouris P. Carbon nanotubes: synthesis, structure, properties, and applications. Topics in applied physics, vol. 80. Berlin: Springer; 2001.
[32] Jorio A, Pimenta MA, Souza Filho AG, Saito R, Dresselhaus G, Dresselhaus MS. New J Phys 2003;5:1–17 [paper no. 139].
[33] Halpin JC, Kardos JL. Polym Eng Sci 1976;16:344.
[34] Halpin JC, Finlayson KM, Ashton JE. Primer on composite materials analysis. 2nd rev/ed. Lancaster, PA: Technomic Pub. Co.; 1992.
[35] Ballard DGH, Burgess AN, Cheshire P, Janke EW, Nevin A, Schelten J. Polymer 1981;22:1353.
[36] Fustin C-A, Bailly C, Clarkson GJ, Galow TH, Leigh DA. Macromolecules 2004;37:66.
[37] Yoon PJ, Hunter DL, Paul DR. Polymer 2003;44:5323.
[38] Terrones M. Annu Rev Mater Res 2003;33:419.
[39] Haggenmueller R, Zhou W, Fischer JE, Winey KI. J Nanosci Nanotechnol 2003;3:105.
[40] Wagner HD, Richard AV. Mater Today 2004;7:38.
[41] Baur JW et al. In preparation.